Hysteresis in transverse galloping: The role of the inflection points

A. Barrero-Gil*, A. Sanz-Andrés, G. Alonso

ETSI Aeronáuticos, Instituto Universitario 'Ignacio Da Riva', Universidad Politécnica de Madrid, E-28040 Madrid, Spain

Abstract

Transverse galloping is here considered as a one-degree-of-freedom oscillator subjected to aerodynamic forces, which are described by using the quasi-steady hypothesis. The hysteresis of transverse galloping is also analyzed. Approximate solutions of the model are obtained by assuming that the aerodynamic and damping forces are much smaller than the inertial and stiffness ones. The analysis of the approximate solution, which is obtained by means of the method of Krylov–Bogoliubov, reveals the existing link between the hysteresis phenomenon and the number of inflection points at the aerodynamic force coefficient curve, $C_y(\alpha)$; C_y and α being, respectively, the force coefficient normal to the incident flow and the angle of attack. The influence of the position of these inflection points on the range of flow velocities in which hysteresis takes place is also analyzed.
© 2009 Elsevier Ltd. All rights reserved.

1. Introduction

Transverse galloping is synonymous with the well-known stall flutter phenomenon in aeronautics; it is a well-known one-degree-of-freedom aeroelastic instability firstly described by Lanchaster (1907). These low frequency self-excited oscillations develop only in structures whose cross-sections are non-circular (Rockwell and Naudascher, 1994). The frequency of the oscillations is approximately the same as the natural frequency of the structure (when the density of the structure is much higher than the air density). The classic example of transverse galloping is the oscillation of the wires of the electric transmission lines that is sometimes observed when ice accretion on the wires modifies their initially almost circular sections. The phenomenon has also been observed in cantilevered traffic signs and signal supports (Johns and Dexter, 1998) or in marine pipelines where the deposition of organic material on the surface of the pipes gives rise to sections with more or less elliptical shapes (Simpson, 1972).

Den Hartog (1956) was the first one in establishing the conditions for the onset of transverse galloping using the quasi-steady hypothesis to describe the linearized aerodynamic forces. Generally, this assumption is justified, since galloping occurs at high flow velocities, so that the characteristic timescale of the flow, $t_r = L/U$, is small compared to the characteristic timescale of the changes in the boundary conditions, which is of the order $t_{cc} = 1/\omega_0$ (ω_0 is the natural

---

*Corresponding author. Tel./fax: +34 913366353.

E-mail address: antonio.barrero@upm.es (A. Barrero-Gil).

frequency of vibration of the structure and L and U are the characteristic length and velocity of the flow), therefore $t_r/t_{cc} = \omega_0 L/U \ll 1$. In this case, the aerodynamic force acting on the oscillating structure is approximately equal to the static aerodynamic force evaluated at the instantaneous angle of attack of the incident flow.

However, the linearized model is not appropriate for describing the time evolution of the structure once galloping is started. To perform this analysis, post-critical, nonlinear terms must be retained. These nonlinear terms limit the amplitude of the oscillations and drive the system towards a limit cycle of oscillations (LCO). Once the LCO has been reached, the energy input to the structure by the flow equals the energy dissipated by structural damping averaged along a cycle. Parkinson (1961, 1964) developed a one-degree-of-freedom nonlinear model where the nonlinear aerodynamic forces were described by the quasi-steady hypothesis (a similar analysis was done by Sisto (1953) in the study of the instabilities in a cascade of turbine blades operating at high angles of attack). Parkinson's analyses not only determined the amplitude of the limit cycle oscillations as a function of the flow velocity, but they also shed light on the hysteresis effect observed in some galloping experiments. In those experiments it was found that after the onset of galloping, multiple solutions for the amplitude of oscillations can appear for a range of flow velocity. In addition, the amplitude of the LCO was different, depending on whether the reduced velocity was increasing or decreasing.

Later, in a number of papers, Novak (1969, 1972) extended the analysis of transverse galloping to the three-dimensional case. He considered structures with rectangular cross-sections and analyzed their different galloping responses. He pointed out that there are four basic types of $C_y(\alpha)$ curves, C_y and α being, respectively, the force coefficient normal to the incident flow and the angle of attack, each one associated with its own characteristic response. Blevins and Iwan (1974) considered the case of a system with two degrees of freedom (vertical and rotational). In this case, the angle of attack induced by the movement depends on both the velocity and the position of the oscillator; therefore, the aerodynamic force has not only a damping effect as in the case of transverse galloping (see Section 2), but there is also an added stiffness effect. Another consequence is that, due to the rotational motion, the application of the quasi-steady hypothesis is less obvious, because an exact equivalent steady situation cannot be defined. Recently, Van Oudheusden (2000) studied the rotational galloping of a square cross-section cylinder. One of the conclusions is a slight disagreement between quasi-steady theory and experiments.

The effects of turbulence on transverse galloping were explored by Novak and Tanaka (1974). They found that turbulence had a stabilizing effect for structures with sections of given shapes, while it was destabilizing for others (they used the intensity of turbulence as the only parameter to describe turbulence). Nakamura and Matsukawa (1987) explored the limits of the quasi-steady hypothesis and Hémon (1999) and Hémon and Santi (2002) gave a correction for the quasi-steady hypothesis by introducing a time delay between the aerodynamic force and the oscillation.

Despite its intrinsic interest, understanding of galloping hysteresis has not received much attention until Luo et al. (2003). These investigators showed that the galloping hysteresis is related to the existence of one, or more, inflection point in the curve of the static aerodynamic coefficient $C_y(\alpha)$. The presence of an inflection point is due to the reattachment of the flow on either the lower or the upper side of the square cylinder (the characteristic shape of the cross-section of the structure considered in Luo et al. paper) as can be deduced from the visualization experiments carried out by Luo and co-workers. One of the objectives of the present paper is to demonstrate unequivocally the link between the emergence of inflection points and the hysteresis phenomenon. Throughout this paper we will demonstrate that the hysteresis phenomenon and the number of LCOs associated with this phenomenon are determined by the number of points of inflection of the curve $C_y(\alpha)$. Indeed, the influence of the position of the points of inflection on the range of fluid velocity where hysteresis takes place is analyzed.

This paper is organized as follows: the mathematical model that describes approximately the phenomenon of transverse galloping is presented in Section 2. Section 3 briefly describes the asymptotic method used to obtain analytical solutions of the mathematical model. The link between the appearance of hysteresis in transverse galloping and the existence of inflection points in the $C_y(\alpha)$ curve is unambiguously shown in Section 4; indeed, we show the influence of the position of the inflection points over the range of flow velocity in which hysteresis takes place. Finally, results are discussed and summarized in Section 5.

2. Mathematical model

The description of the behaviour of a structure under the action of an incident flow is an extremely complex problem; therefore, its modelling must be conveniently simplified for making the analysis more affordable. The assumptions that (i) the structure is described as a linear oscillator of one degree of freedom, (ii) the structure is sufficiently slender to consider two-dimensional flow, and (iii) that the incident flow is free of turbulence are rather common simplifications in the fluid–structure interaction analysis. Under these conditions, the equation governing the dynamics of the transverse
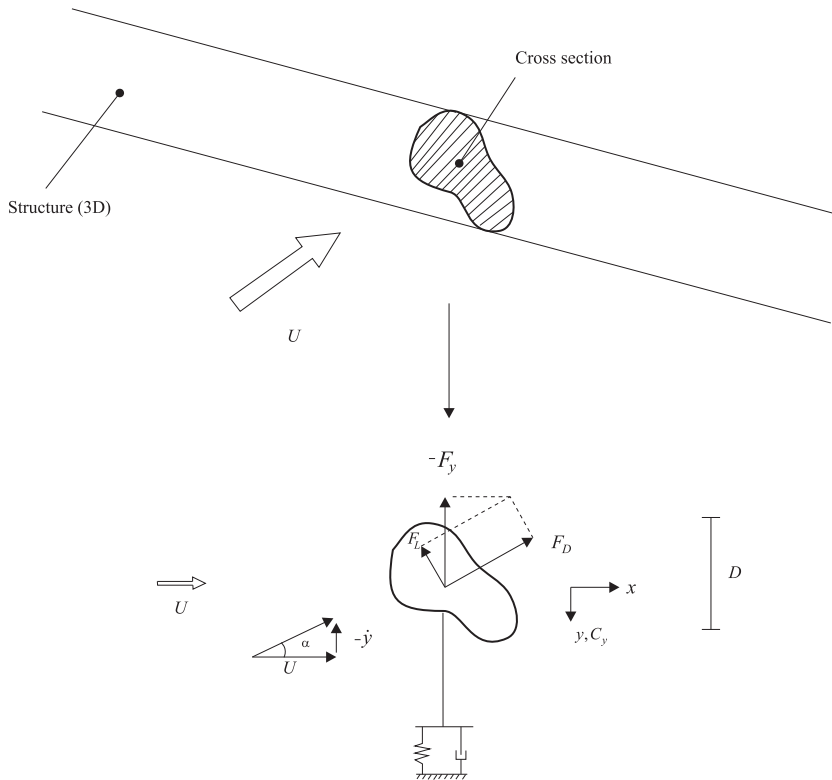
Fig. 1. Schematic representation of the aerodynamic forces and the induced angle of attack by means of the quasi-steady hypothesis.

galloping is (see sketch in Fig. 1)

$$m(\ddot{y} + 2\zeta_y \omega_y \dot{y} + \omega_y^2 y) = F_y = \tfrac{1}{2}\rho U^2 D C_y, \tag{1}$$

where y denotes the vertical position, m is the mass of the structure per unit length, ζ_y is the dimensionless structural damping coefficient, ω_y is the undamped natural frequency, ρ is the fluid density, which will be considered constant throughout the analysis, U is the velocity of the incident flow, D is the characteristic dimension of the structure in the direction of the flow, C_y is the dimensionless coefficient of the aerodynamic force in the normal direction to the incident flow; finally, the dot symbol stands for differentiation with respect to time t.

As advanced in the Introduction, the aerodynamic force will be evaluated by resorting to the quasi-steady assumption, whose use is justified because

(i) the characteristic timescale of the structure oscillations is much larger than the characteristic timescale of the flow,
(ii) the vortex shedding frequency is much higher than the oscillation frequency of the structure.

Thus, the aerodynamic force is completely determined by the instantaneous position of the structure; inertial and memory effects are considered to be of lower order, so that aerodynamic force data in the static case can be used, and they can easily be related to the motion of the structure.

In the static case, the force coefficient perpendicular to the incident flow can be expanded in powers of the angle of attack, α, in the range of interest, $[-\alpha^*, \alpha^*]$, α^* being moderately small,

$$C_y(\alpha) = \sum_{j=0}^{n} a_j \alpha^j, \tag{2}$$

where α is the angle between the incident flow and the reference direction (in the static equilibrium position of the structure, see Fig. 1).

Assuming small values of the velocity ratio $\dot{y}/U$ and expanding α in Taylor series, $\alpha = \arctan(\dot{y}/U) \simeq \dot{y}/U$, one obtains

$$C_y(\alpha) = \sum_{j=0}^{n} a_j \left(\frac{\dot{y}}{U}\right)^j. \tag{3}$$

Then, Eq. (1) can be rewritten as

$$m(\ddot{y} + 2\zeta_y \omega_y \dot{y} + \omega_y^2 y) = \frac{1}{2}\rho U^2 D \sum_{j=0}^{n} a_j \left(\frac{\dot{y}}{U}\right)^j. \tag{4}$$

Introducing dimensionless variables $\eta = y/D$ and $\tau = \omega_y t$ and the reduced velocity $U_r = U/\omega_y D$, Eq. (4) becomes

$$\eta'' + 2\zeta_y \eta' + \eta = \mu U_r^2 \sum_{j=0}^{n} a_j \left(\frac{\eta'}{U_r}\right)^j, \tag{5}$$

where the prime represents differentiation with respect to the dimensionless time τ and $\mu = \rho D^2/2m$ is the dimensionless mass ratio.

For $j \geq 2$, Eq. (5) is an autonomous nonlinear ordinary differential equation. Obviously, if we retain only the first term of the expansion, Den Hartog's result is recovered and the critical reduced velocity of galloping is given by $U_{rg} = 2\zeta_y/\mu a_1$; clearly, results are physically relevant only for $a_1 > 0$. Once the function $C_y(\alpha)$ is known, Eq. (5) can be solved either numerically or by asymptotic methods if the nonlinear term is small. In the case that both aerodynamic and damping forces, of order of μU_r and ζ_y, respectively, are small compared with inertia and stiffness forces (of order of unity in the dimensionless equation), solutions of Eq. (5) will tend to a limit cycle of quasi-harmonic oscillations. This behaviour of the structure is quite usual if its mean density is much higher than that of the fluid (for air, μ is typically of order 10^{-3} and $\mu U_r \sim 10^{-2}$) and the value of the structural damping coefficient rarely exceeds 1%.

Another consequence is that only the antisymmetric part of $C_y(\alpha)$ plays a relevant role in the dynamics. Actually, the aerodynamic work in an oscillation cycle can be expressed as

$$\int_0^T F_y \dot{y} \, dt = \frac{1}{2}\rho U^2 D \int_0^T C_y \dot{y} \, dt,$$

where $C_y = \sum_{j=0}^{n} a_j (\dot{y}/U)^j$, and T states for a one full period. Obviously, under harmonic oscillations, only the terms with odd powers in the polynomial $C_y(\alpha)$ yield nonzero contributions to the integral. In the following, we consider weak aerodynamic forces and that in the polynomial expression for $C_y(\alpha)$ only odd terms are retained.

3. Asymptotic solutions: Krylov–Bogoliubov method

The main advantage of the approximate solutions of nonlinear differential equations in comparison to the numerical solution is that in the former case it is easier to study the role of the different parameters. Perturbation (or asymptotic) methods, as, for example, the Krylov–Bogoliubov method (Murdock, 1991), are particularly useful to obtain approximate solutions for weakly nonlinear oscillators. Let us present a brief summary. Consider the nonlinear harmonic oscillator

$$\ddot{x} + x = \varepsilon f(x, \dot{x}), \quad \varepsilon \ll 1, \tag{6}$$

whose solution for the case $\varepsilon = 0$ is $x(\tau) = X \cos(\tau + \phi)$ (note that in this case overdot denotes differentiation with respect to the dimensionless time τ). For small values of ε, solutions of Eq. (6) can be written as $x(\tau) = X(\tau) \cos[\tau + \phi(\tau)]$, where $X(\tau)$ and $\phi(\tau)$ are the functions slowly varying with τ (the effect of the forcing term is small, giving rise to a slow change of the parameters in the harmonic solution). As the nonlinearity is small, two different timescales exist in the problem, corresponding to the oscillation and the growth of the amplitude of oscillation (their derivatives with respect of τ being of the order of ε). Then, if $x(\tau) = X(\tau) \cos[\tau + \phi(\tau)]$, its derivative with respect to τ taking into account that $\dot{X} \sim \dot{\phi} \ll 1$ is

$$\dot{x}(\tau) = -X \sin[\tau + \phi(\tau)], \tag{7}$$

with the additional condition

$$\dot{X} \cos[\tau + \phi(\tau)] - X \dot{\phi} \sin[\tau + \phi(\tau)] = 0. \tag{8}$$

Introducing the derivative of (7) with regard to τ into Eq. (6), one finds at the lowest order

$$\dot{X}\sin[\tau+\phi(\tau)] - X\dot{\phi}\cos[\tau+\phi(\tau)] = \varepsilon f[X\cos(\tau+\phi), -X\sin(\tau+\phi)], \tag{9}$$

which together with condition (8) yields

$$\dot{X} = -\frac{\varepsilon}{2\pi}\int_0^{2\pi} f[X\cos(\tau+\phi), -X\sin(\tau+\phi)]\sin(\tau+\phi)\,d\tau,$$

$$\dot{\phi} = -\frac{\varepsilon}{2\pi X}\int_0^{2\pi} f[X\cos(\tau+\phi), -X\sin(\tau+\phi)]\cos(\tau+\phi)\,d\tau.$$

Applying this method to Eq. (5), we look for solutions in the form

$$\eta = r(\tau)\cos[\tau+\phi(\tau)], \quad \eta' = -r(\tau)\sin[\tau+\phi(\tau)] + \mathcal{O}(r'),$$

where r and ϕ vary slowly with τ. The application of the Krylov–Bogoliubov method leads to

$$r' = -\frac{1}{2\pi}\int_0^{2\pi}\left(-2\zeta_y\eta' + \mu U_r^2 \sum_{j=0}^n a_j\left(\frac{\eta'}{U_r}\right)^j\right)\sin(\tau+\phi)\,d\tau. \tag{10}$$

The evaluation of (10) is straightforward because $\eta' = -r\sin(\tau+\phi)$ during a cycle of oscillation ($0 \leq \tau \leq 2\pi$) (r and ϕ are constants); therefore, the integrand is composed of terms which are proportional to the powers of $\sin(\tau+\phi)$. Integrating by parts, it is easily shown that a recurrence relation appears and

$$\frac{1}{2\pi}\int_0^{2\pi}(\sin x)^{j+1}\,dx = k_j = \frac{j}{j+1}k_{j-2}, \quad j = 3,5,7,9,\ldots, \quad (k_1 = 1/2)$$

$$\frac{1}{2\pi}\int_0^{2\pi}(\sin x)^{j+1}\,dx = 0, \quad j = 2,4,6,8,\ldots,$$

and therefore,

$$r' = -\zeta_y r + \mu\sum_j\left(\frac{a_j}{U_r^{j-2}}k_j\right)r^j, \tag{11}$$

where $j = 1,3,5,7,9,\ldots$ and $k_{-1} = 1$.

It is noteworthy that for large values of j, k_j remains small. Since U_r is large compared to unity (quasi-steady hypothesis), the series in Eq. (11) is convergent unless $a_j/U_r^{j-2} \gg 1$, which has no physical meaning (see Fig. 2).
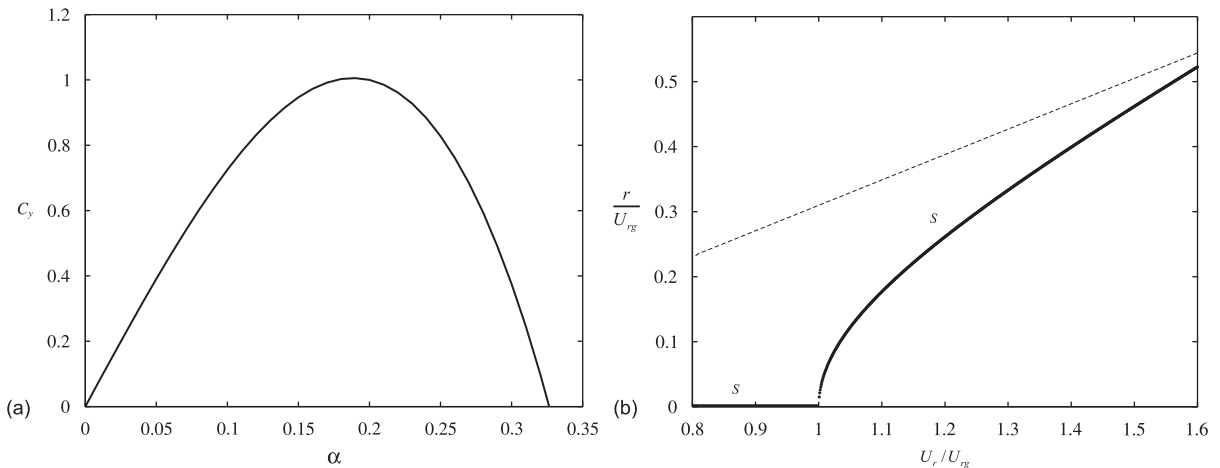

(a)

(b)

Fig. 2. (a) Static curve of C_y with no inflection points. $C_y = 8\alpha - 75\alpha^3$. (b) Universal response to galloping with C_y data obtained by the Krylov–Bogoliubov method; —, universal response to galloping; ----, asymptotic character of the solution when $U_r/U_{rg} \gg 1$.

Now, the advantage of the approximate solution of Eq. (5) is clear, because thanks to the functional relationship obtained in (11), $r' = F(r, \mu, \zeta_y, U_r, a_j)$, it is easy to determine the amplitude(s) of the limit cycle(s) as a function of the flow velocity, mass ratio, structural damping and the coefficients a_j of the static force coefficient C_y. Amplitudes of LCO(s) are given by the real and positive roots of $r' = 0$ [$F(r, \mu, \zeta_y, U_r, a_j) = 0$], and the stability analysis shows that the LCO is stable if

$$\left.\frac{\mathrm{d}F(r, \zeta_y, U_r, a_j)}{\mathrm{d}r}\right|_{r=r^*} < 0,$$

r^* being the amplitude of the LCO.

4. Influence of the shape of the C_y curve on the hysteresis phenomenon

As we pointed out in the Introduction, the hysteresis region is characterized by the existence of a solution that can alternately reach different cycles limits. In this case, the characteristic polynomial that provides the amplitude of the LCO, $F(r, \mu, \zeta_y, U_r, a_j) = 0$, presents more than a real positive solution.

In the following, let us analyze the solutions corresponding to a variety of $C_y(\alpha)$ curves typical of bluff bodies in order to clarify the correlation between the number of inflection points and the hysteresis. Indeed, we study the role of the position of these inflection points over the range of hysteresis. Since the galloping dynamics is unaffected by the even terms of the polynomial $C_y(\alpha)$, we have only considered antisymmetric polynomials.

4.1. $C_y(\alpha)$ curve with no inflection points

The minimum order of an antisymmetric polynomial which do not exhibit inflection points ($\alpha_i > 0$) is three, so that C_y is given by

$$C_y(\alpha) = a_1 \alpha + a_3 \alpha^3, \quad \alpha > 0. \tag{12}$$

Substituting (12) in Eq. (11), one obtains the average equation for the amplitude

$$r' = F(r) = \left(-\zeta_y + \frac{\mu a_1 U_r}{2}\right)r + \frac{3}{8}\mu a_3 \frac{1}{U_r}r^3. \tag{13}$$

We define next appropriate dimensionless variables, as suggested by Novak (1969), $r^* = \mu a_1 r / 2\zeta_y$ for the amplitude of the oscillation and the flow velocity parameter $U_r^* = \mu a_1 U_r / 2\zeta_y = U_r / U_{rg}$ (here U_{rg} is the critical reduced velocity of galloping). Note that through this normalization, all response curves collapse to a universal curve irrespective of differences in mass and structural damping, and one gets

$$\left(-\zeta_y + \frac{\mu a_1 U_r}{2}\right)r = \frac{\mu a_1}{2}(U_r^* - 1)U_{rg}^2 r^*, \quad \frac{3}{8}\mu a_3 \frac{1}{U_r}r^3 = \frac{3}{8}\mu a_3 \frac{1}{U_r^*}U_{rg}^2 r^{*3}, \quad r' = U_{rg}r^{*'}.$$

Then, Eq. (13) can be written as

$$r^{*'} = F(r^*) = U_{rg}\left(\frac{\mu a_1}{2}(U_r^* - 1)r^* + \frac{3}{8}\mu a_3 \frac{1}{U_r^*}r^{*3}\right), \tag{14}$$

and

$$r^{*''} = \mathrm{d}F(r^*)/\mathrm{d}r^* = U_{rg}\left(\frac{\mu a_1}{2}(U_r^* - 1) + \frac{9}{8}\mu a_3 \frac{1}{U_r^*}r^{*2}\right). \tag{15}$$

The LCO(s) is (are) given by the real and positive roots of $F(r^*) = 0$ and its (their) stability is governed by the sign of the gradient $r^{*''} = \mathrm{d}F(r^*)/\mathrm{d}r^*$ evaluated at LCO. Therefore, from Eq. (14) the roots are

$$\text{(i)} \ r_1^* = 0, \quad \text{(ii)} \ r_2^* = \left(-\frac{4a_1}{3a_3}(U_r^* - 1)U_r^*\right)^{1/2}.$$

If $a_1 > 0$ (galloping criterion) the solution of $r_1^{*'} = 0$ becomes unstable for $U_r^* \geq 1$ and jumps to a stable LCO with amplitude given by r_2^* if $a_3 < 0$. The evolution of r^* as a function of U_r^* is shown in Fig. 2. Observe that there is no hysteresis in a galloping driven by a $C_y(\alpha)$ curve without inflection points.

4.1.1. $C_y(\alpha)$ curve with one inflection point

The minimum order of an antisymmetric polynomial which exhibit one inflection point $(\alpha_i > 0)$ is five, so that C_y is given by

$$C_y(\alpha) = a_1\alpha + a_3\alpha^3 + a_5\alpha^5, \quad \alpha > 0.$$

For $a_3/a_5 < 0$, this curve has an inflection point at $\alpha_i = (-3a_3/10a_5)^{1/2}$. Proceeding in identical form than in the previous case, one gets the dimensionless average amplitude

$$r^{*'} = F(r^*) = U_{rg}\left(\frac{\mu a_1}{2}(U_r^* - 1)r^* + \frac{3}{8}\mu a_3 \frac{1}{U_r^*}r^{*3} + \frac{5}{16}\mu a_5 \frac{1}{U_r^{*3}}r^{*5}\right),$$

and the gradient

$$r^{*''} = dF(r^*)/dr^* = U_{rg}\left(\frac{\mu a_1}{2}(U_r^* - 1) + \frac{9}{8}\mu a_3 \frac{1}{U_r^*}r^{*2} + \frac{25}{16}\mu a_5 \frac{1}{U_r^{*3}}r^{*4}\right).$$

The LCO(s) are given by the real and positive roots of $F(r^*) = 0$. This means

$$F(r^*) = r^* U_{rg}(A + BY + CY^2) = 0, \tag{16}$$

where we denoted $Y = r^{*2}$, $A = \frac{1}{2}\mu a_1(U_r^* - 1)$, $B = \frac{3}{8}\mu a_3/U_r^*$ and $C = \frac{5}{16}\mu a_5/U_r^{*3}$. As $r^* > 0$, the quadratic polynomial should vanish. Therefore, the amplitude of LCO(s) is given by the roots of (16)

$$Y = -\frac{B}{2C} \pm \frac{(B^2 - 4AC)^{1/2}}{2C},$$

which are both real if $B^2 - 4AC > 0$, and positive if $-B/2C > 0$ and $AC > 0$. Note that

 (i) $-B/2C > 0$ implies that $a_3/a_5 < 0$; as shown before, this condition is satisfied if C_y presents an inflection point;
 (ii) $4AC > 0$ implies that $U_r^* < 1$ for $a_1 a_5 < 0$ ($U_r^* > 1$ for $a_1 a_5 > 0$);
 (iii) condition $B^2 - 4AC > 0$ yields the other limit for U_r^* of the hysteresis region:

   (a) $0 < -\dfrac{40a_1 a_5}{9a_3^2 - 40a_1 a_5} < U_r^* < 1 \ (a_1 a_5 < 0),$

   (b) $1 < -\dfrac{40a_1 a_5}{9a_3^2 - 40a_1 a_5} < U_r^* \ (a_1 a_5 > 0, 9a_3^2 - 40a_1 a_5 < 0).$ \hfill (17)

It should be pointed out that the same result is obtained if one determines the point of the saddle–node bifurcation (considered here as the point where the character of LCO changes from unstable to stable and the gradient $r^{*''}$ takes a zero value). In fact, if Eq. (16) provides the amplitudes of LCO(s), then the saddle–node point is given by the condition $B + 2CY = 0$,

$$Y_{SN} = r_{SN}^{*2} = -3a_3 U_r^{*2}/5a_5 = 2\alpha_i^2 U_r^{*2},$$

which is acceptable only if $a_3/a_5 < 0$ (condition of existence of an inflection point). Introducing this result in Eq. (16), one arrives at the same result than above (Eq. (17)):

$$U_r^*|_{SN} = -\frac{40a_1 a_5}{9a_3^2 - 40a_1 a_5} = \frac{1}{(3a_3/4a_1)\alpha_i^2 + 1}. \tag{18}$$

It is interesting to note that this last expression allows to determine the sensitivity with regard to the position of the point of saddle–node bifurcation, and, therefore, the range of hysteresis as a function of the coefficients of the $C_y(\alpha)$ polynomial. In effect, taking the first derivatives of expression (18) with respect to the three coefficients a_1, a_3 and a_5,

$$\frac{\partial U_r^*|_{SN}}{\partial a_1} = -\frac{360a_3^2 a_5}{(9a_3^2 - 40a_1 a_5)^2}, \quad \frac{\partial U_r^*|_{SN}}{\partial a_3} = \frac{720a_1 a_3 a_5}{(9a_3^2 - 40a_1 a_5)^2}, \quad \frac{\partial U_r^*|_{SN}}{\partial a_5} = -\frac{360a_3^2 a_1}{(9a_3^2 - 40a_1 a_5)^2},$$

one arrives at the following conclusions (see Fig. 3(a)):

 (i) if $a_5 < 0$, then $\partial U_r^*|_{SN}/\partial a_1 > 0$. In this case, the larger is a_1 the narrower will be the hysteresis region; note that $U_r^*|_{SN}$ increases with a_1;
 (ii) if $a_5 < 0$, then $\partial U_r^*|_{SN}/\partial a_3 < 0$; therefore, the hysteresis region is wider since $U_r^*|_{SN}$ decreases as a_3 increases;
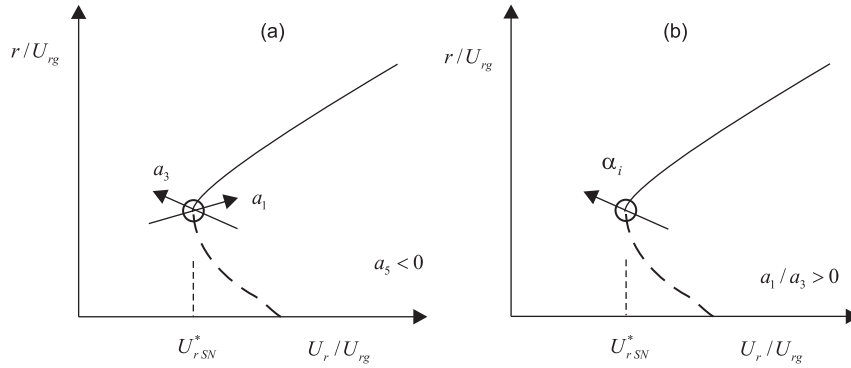
Fig. 3. Range of hysteresis when C_y exhibits one inflection point: (a) dependence with regard to the coefficients and (b) with respect to the position of the inflection point.

(iii) $\partial U_r^*|_{SN}/\partial a_5 < 0$; therefore if a_5 increases the interval of the hysteresis region increases too, since $U_r^*|_{SN}$ decreases when a_5 increases.

From Eq. (18) a new interesting aspect appears: the position of the point of inflection has influence in the size of the hysteresis region. Taking the first derivatives of expression (18) with respect to α_i,

$$\frac{\partial U_r^*|_{SN}}{\partial \alpha_i} = -\frac{(3a_3/2a_1)\alpha_i}{\left((3a_3/4a_1)\alpha_i^2 + 1\right)^2},$$

one arrives at the following conclusion (see Fig. 3(b)): if $a_3/a_1 > 0$ then $\partial U_r^*|_{SN}/\partial \alpha_i < 0$, i.e. the further the inflection point is from the origin the wider the hysteresis region is; however, when $a_3/a_1 < 0$ then $\partial U_r^*|_{SN}/\partial \alpha_i > 0$.

Fig. 4 shows the results of a parametric study on the size of hysteresis region where some coefficients of $C_y(\alpha)$ are properly varied. From the study shown in the figure we can deduce some conclusions summarized in Table 1. Table 2 shows the value of coefficients of $C_y(\alpha)$ used for the study and the position of the inflection point, α_i. The results indicate the expected dependence. Fig. 5 shows the universal response of the system to a $C_y(\alpha)$ curve with one inflection point. Observe that there is a hysteresis region for the interval $U_r^*|_{SN} < U_r^* < 1$ and just one LCO for $U_r^* \geq 1$.

4.2. $C_y(\alpha)$ curve with two inflection points

The minimum order of an antisymmetric polynomial which exhibits two inflection points ($\alpha_{i1}, \alpha_{i2} > 0$) is seven, so that C_y is given by

$$C_y(\alpha) = a_1\alpha + a_3\alpha^3 + a_5\alpha^5 + a_7\alpha^7, \quad \alpha > 0.$$

This curve has two inflection points given by

$$\alpha_{i1,i2} = \left(-\frac{20a_5}{84a_7} \pm \frac{1}{84a_7}(400a_5^2 - 1008a_3a_7)^{1/2}\right)^{1/2},$$

which are real and positive if both $a_3/a_7 > 0$ and $a_5/a_7 < 0$. Dimensionless average amplitude may be obtained by proceeding in identical form than in the previous case; then, we arrive at

$$r^{*'} = F(r^*) = U_{rg}\left(\frac{\mu a_1}{2}(U_r^* - 1)r^* + \frac{3}{8}\mu a_3 \frac{1}{U_r^*}r^{*3} + \frac{5}{16}\mu a_5 \frac{1}{U_r^{*3}}r^{*5} + \frac{35}{128}\mu a_7 \frac{1}{U_r^{*5}}r^{*7}\right),$$

and the gradient

$$r^{*''} = dF(r^*)/dr^* = U_{rg}\left(\frac{\mu a_1}{2}(U_r^* - 1) + \frac{9}{8}\mu a_3 \frac{1}{U_r^*}r^{*2} + \frac{25}{16}\mu a_5 \frac{1}{U_r^{*3}}r^{*4} + \frac{245}{128}\mu a_7 \frac{1}{U_r^{*5}}r^{*6}\right).$$

The real and positive roots of $F(r^*) = 0$ yield the amplitude of LCO(s); so that

$$r^* U_{rg}\left(A + BY + CY^2 + DY^3\right) = 0. \tag{19}$$

The analysis of (19) shows the existence of three different solutions separated by two saddle–node bifurcation points
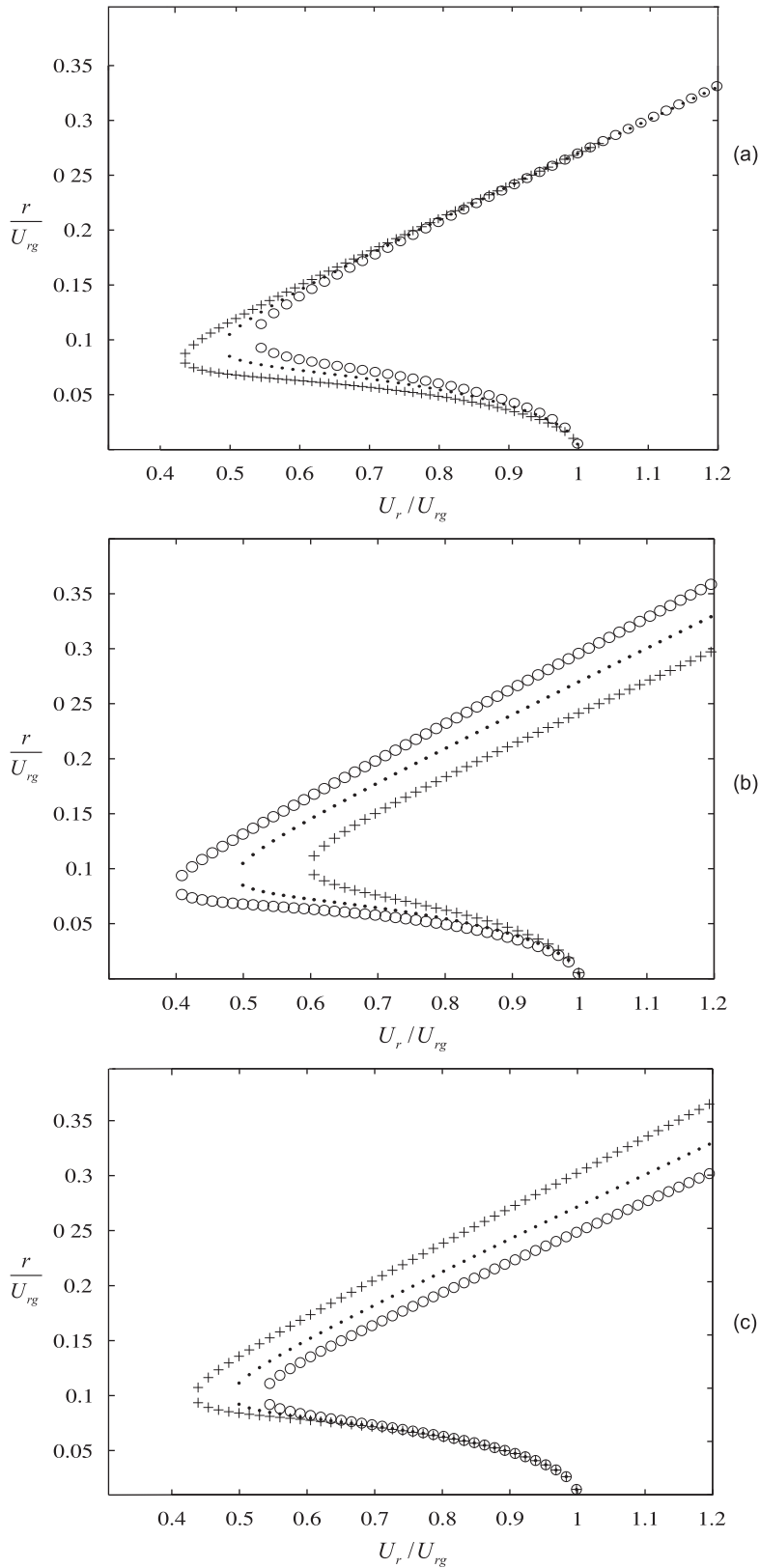
Fig. 4. Influence of the (a) a_1, (b) a_3, and (c) a_5 coefficients in the hysteresis range. The values of a_1, a_3 and a_5 are given in Table 2.

Table 1
Influence in the range of hysteresis of the coefficients of $C_y(\alpha)$.

$\triangle U_{rh}^*/ \triangle |a_1|$	$\triangle U_{rh}^*/ \triangle |a_3|$	$\triangle U_{rh}^*/ \triangle |a_5|$
<0	>0	<0

U_{rh}^* is the range of flow velocity where hysteresis takes place.

Table 2
Coefficients of the static curve $C_y = a_1\alpha + a_3\alpha^3 + a_5\alpha^5$ used to get the universal response shown in Fig. 4.

id	(a)				(b)				(c)			
	a_1	a_3	a_5	α_i	a_1	a_3	a_5	α_i	a_1	a_3	a_5	α_i
·	$1.5 = x$	231	−3800	0.13	1.5	$231 = y$	−3800	0.13	1.5	231	$-3800 = z$	0.13
○	$1.2x$	231	−3800	0.13	1.5	$1.2y$	−3800	0.15	1.5	231	$1.2z$	0.12
+	$0.8x$	231	−3800	0.13	1.5	$0.8y$	−3800	0.12	1.5	231	$0.8z$	0.15

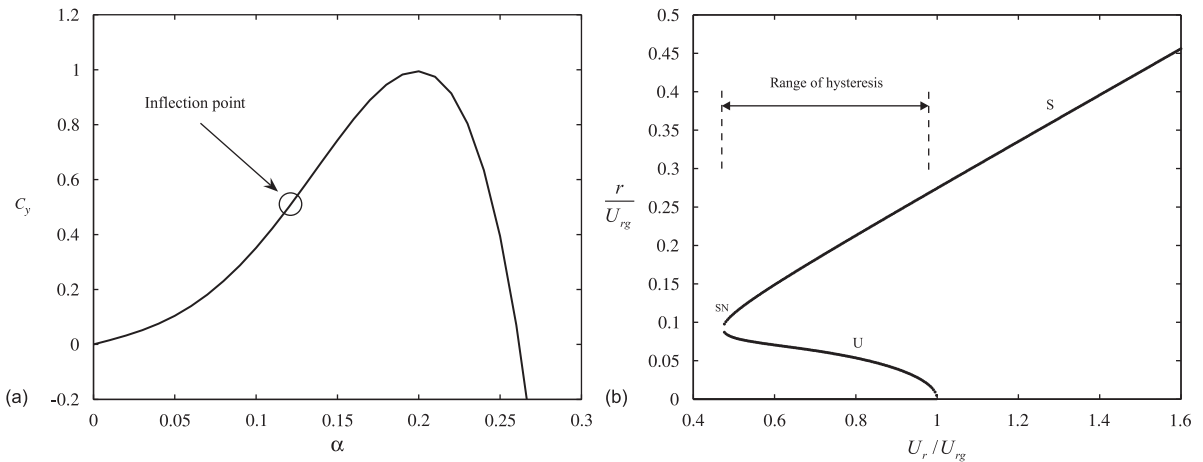$\langle\langle id \rangle\rangle$ is used to identify the corresponding responses shown in Fig. 6.

Fig. 5. (a) Static curve of C_y with one inflection point. $C_y = 1.5\alpha + 238\alpha^3 - 3800\alpha^5$. (b) Universal response to galloping with C_y data obtained by the Krylov–Bogoliubov method. U: unstable, S: stable, SN: saddle–node.

given by

$$Y_{SN1,SN2} = -\frac{4}{105}\left(\frac{10a_5 \pm (100a_5^2 - 315a_3a_7)^{1/2}}{a_7}\right)U_r^{*2}. \tag{20}$$

These solutions, which are real and positive if both $a_3/a_7 > 0$ and $a_5/a_7 < 0$, show again the link between the number of inflection points in $C_y(\alpha)$ and the number of LCO(s) in the hysteresis region. The response of the system to a $C_y(\alpha)$ curve with two inflection points is given in Fig. 6. Observe that the appearance of two inflection points brings a hysteresis phenomenon with three LCOs. Let us now discuss the extent of the flow velocity range in which the hysteresis phenomenon appears. In this case the algebra is more complicated and we have carried out a numerical parametric study where some coefficients of $C_y(\alpha)$ have been properly varied. Fig. 7 shows the results of the study; we can deduce some conclusions summarized in Table 3. Table 4 shows the value of coefficients of $C_y(\alpha)$ used for the study and Table 5
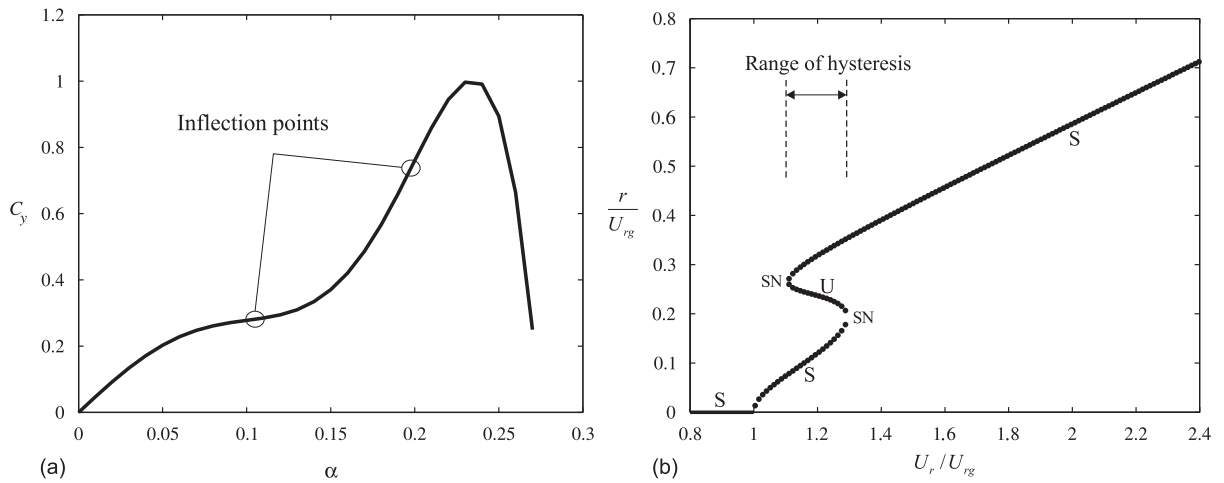
Fig. 6. (a) Static curve of C_y with two inflection points. $C_y = 4.72\alpha - 294\alpha^3 + 10\,972\alpha^5 - 105\,000\alpha^7$. (b) Universal response to galloping with C_y data obtained by the Krylov–Bogoliubov method. U: unstable, S: stable, SN: saddle–node.
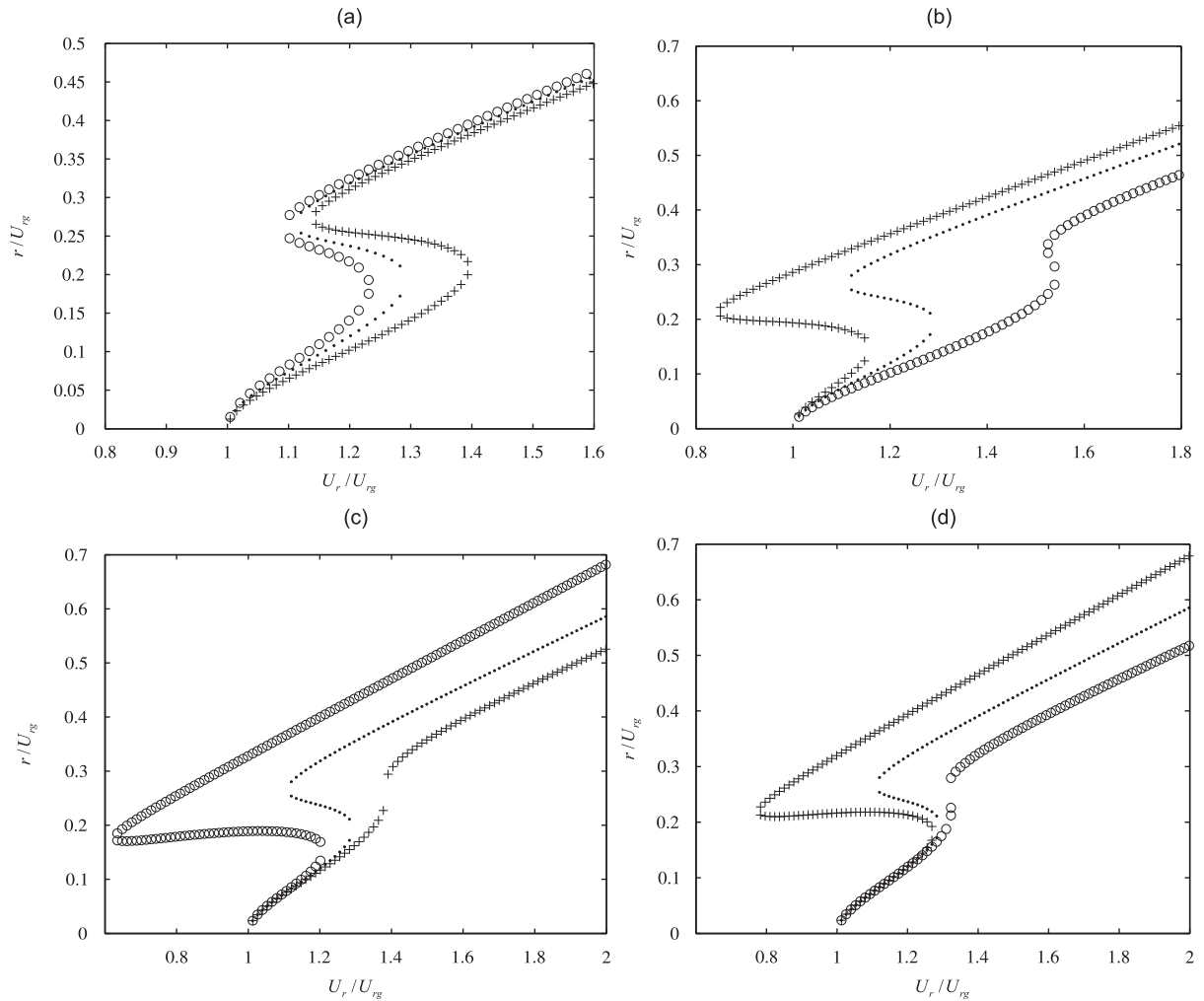

Fig. 7. Influence of the (a) a_1, (b) a_3, (c) a_5, and (d) a_7 coefficients in the hysteresis range. In all cases, values for a_1, a_3, a_5 and a_7 are givne in Table 4.

Table 3
Influence in the range of hysteresis of the coefficients of $C_y(\alpha)$.

$\triangle U_{rh}^* / \triangle |a_1|$	$\triangle U_{rh}^* / \triangle |a_3|$	$\triangle U_{rh}^* / \triangle |a_5|$	$\triangle U_{rh}^* / \triangle |a_7|$
<0	<0	>0	<0

U_{rh}^* is the range of flow velocity where hysteresis takes place.

Table 4
Coefficients of the static curve $C_y = a_1\alpha + a_3\alpha^3 + a_5\alpha^5 + a_7\alpha^7$ used to get the universal response shown in Fig. 7.

id	(a)				(b)			
	a_1	a_3	a_5	a_7	a_1	a_3	a_5	a_7
.	$2.7 = x$	-168	6270	$-60\,000$	2.7	$-168 = y$	6270	$-60\,000$
○	$1.2x$	-168	6270	$-60\,000$	2.7	$1.2y$	6270	$-60\,000$
+	$0.8x$	-168	6270	$-60\,000$	2.7	$0.8y$	6270	$-60\,000$

id	(c)				(d)			
	a_1	a_3	a_5	a_7	a_1	a_3	a_5	a_7
.	2.7	-168	$6270 = z$	$-60\,000$	2.7	-168	6270	$-60\,000 = w$
○	2.7	-168	$1.2z$	$-60\,000$	2.7	-168	6270	$1.2w$
+	2.7	-168	$0.8z$	$-60\,000$	2.7	-168	6270	$0.8w$

$\langle\langle id \rangle\rangle$ is used to identify the corresponding responses shown in Fig. 7. $a_1 = 2.7$, $a_3 = -168$, $a_5 = 6270$, and $a_7 = -60000$ correspond to those coefficients obtained experimentally by Novak for a square section (Blevins, 1990, p. 115).

Table 5
Position of the inflection points, α_{i1} α_{i2}, of C_y curves used to get the universal responses shown in Fig. 7. Cases (a), (b) and (c) in the Table correspond to the response shown in Fig. 7(b), (c) and (d), respectively.

id	(a)				(b)				(c)			
	α_{i1}	α_{i2}	$\alpha_{i2} - \alpha_{i1}$	RH	α_{i1}	α_{i2}	$\alpha_{i2} - \alpha_{i1}$	RH	α_{i1}	α_{i2}	$\alpha_{i2} - \alpha_{i1}$	RH
.	0.10	0.19	0.09	R	0.10	0.19	0.09	R	0.10	0.19	0.09	R
○	0.12	0.19	0.07	m	0.08	0.23	0.15	M	0.10	0.17	0.07	m
+	0.08	0.20	0.12	M	0.11	0.18	0.07	m	0.09	0.22	0.13	M

RH≡ Range of hysteresis; R≡ reference value; M≡ major; m≡ minor.

the location of points of inflection. The results presented in Table 5 show that a relationship between the separation of points of inflection and the size of the region of hysteresis can exist.

The shape of the $C_y(\alpha)$ curve depends on the geometry of the body and the initial orientation of that body with respect to the incident flow (i.e. the initial angle of attack before oscillations occur). For some interesting geometries from the point of view of their potential application to actual engineering problems, the variation of $C_l(\alpha)$ and $C_d(\alpha)$ for the whole range $0° < a < 360°$ has been obtained experimentally: biconvex and rhomboidal sections in Alonso et al. (2008). Those coefficients were used to determine galloping stability regions according to the Den Hartog criterion. But also from those aerodynamic coefficients it is easy to determine the $C_y(\alpha)$ curve from an initial angle of attack. Plotting the antisymmetric part of that curve, and looking at the number and position of the inflection points, the analysis presented in this paper can be applied to determine regions of hysteresis in the galloping phenomenon for the respective bodies and initial angles of attack. See Fig. 8 for an example of a $C_y(\alpha)$ curve obtained experimentally. Finally, Table 6
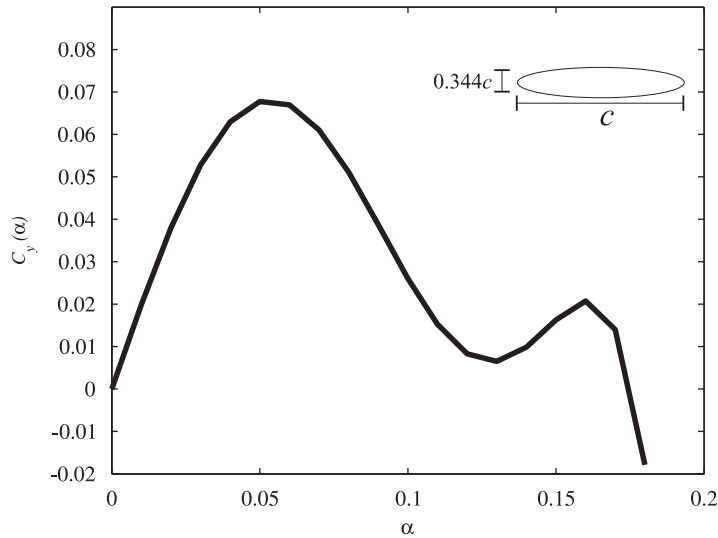
Fig. 8. $C_y(\alpha)$ obtained experimentally by Alonso et al. (2008) for a biconvex cross-section.

Table 6
Summary of the number of LCO as a function of the sign of the coefficients of $C_y(\alpha)$.

a_1	a_3	a_5	a_7	a_9	N	sg(a_1) = sg(a_3)	N_p	N_{LCO}	Type of excitation
+	−				1	No	0	1	Soft
+	+	−			1	Yes	1	2	Hard
−	+	−			2	No	1	2	Hard
+	−	+	−		3	No	2	3	Soft
−	+	−	+	−	4	No	3	4	Hard

N is the number of sign changes in the list of coefficients. N_p is the number of inflection points. N_{LCO} is the number of LCO in the response. Observe that $N_{LCO} = N_p + 1$. Note that we present here only cases with physical meaning.

presents a summary of the different cases that can appear as a function of the different signs in the list of coefficients of $C_y(\alpha)$.

5. Conclusions

Transverse galloping has been analyzed as a nonlinear oscillator of one degree of freedom. Nonlinear aerodynamic forces limit the amplitude of the transverse galloping oscillations and sometimes lead the oscillator towards a limit cycle, which is calculated by using the quasi-steady assumption. When the aerodynamic forces are relatively weak, it is possible to approximately solve the equation of motion by means of asymptotic techniques that allow for a quick and easy way to determine the amplitude of LCO(s) as a function of the static aerodynamic characteristics, structural properties and flow velocity. The amplitude of LCO(s) are the fixed points of the fist order nonlinear averaged equation obtained with the method of Krylov–Bogoliubov. Two cases, with one and two inflection points, have been solved analytically. The cases of $C_y(\alpha)$ curves with three or more inflection points have not been considered, not only because of the complex algebra of the problem but also because it seems rather unlikely that $C_y(\alpha)$ has three or more inflection points. The influence of the position of the inflection points on the galloping can be deduced from the analysis. For example: in the case that $C_y(\alpha)$ has a unique inflection point, the hysteresis region broadens (the range of velocities for which hysteresis exists increases) when the distance from the inflection point to the origin increases; if $C_y(\alpha)$ presents two inflection points, the interval of flow velocities where hysteresis takes place increases when the separation between inflection points increases too.

The analysis also allows to determine the qualitative behaviour of the oscillator response by a simple inspection of the static aerodynamic data. For example, if one observes the existence of only one inflection point at the $C_y(\alpha)$ curve, then one can automatically deduce that the oscillator may present hysteresis via a subcritical bifurcation (Fig. 3). Moreover, some information about the magnitude of the hysteresis region can be obtained from the location of the inflection point. It should also be emphasized that the qualitative behaviour of the response to galloping and the number of limit cycles are independent of the number of terms of the polynomial used to fit the aerodynamic data whenever the former reproduces all the inflection points of the latter curve.

Acknowledgement

References

Alonso, G., Valero, E., Meseguer, J., 2008. An analysis on the dependence on cross section geometry of galloping stability of two-dimensional bodies having either biconvex or rhomboidal cross sections. European Journal of Mechanics—B/Fluids 28 (2), 328–334.

Blevins, R.D., 1990. Flow-Induced Vibration. Krieger Publishing Company, Florida.

Blevins, R.D., Iwan, W.D., 1974. The galloping response of a two-degree-of-freedom system. Journal of Applied Mathematics 41, 1113–1118.

Den Hartog, J.P., 1956. Mechanical Vibrations. McGraw-Hill, New York.

Hémon, P., 1999. Approche du phenomène de gallop par un modèle déffort retardé et validation expérimentale, Comptes-Rendus de l'Académie des Sciences, Paris, 327, serie II, 679–684.

Hémon, P., Santi, F., 2002. On the aeroelastic behaviour of rectangular cylinders in cross-flow. Journal of Fluids and Structures 16, 855–889.

Johns, K.W., Dexter, R.J., 1998. The development of fatigue design load ranges for cantilevered sign and signal support structures. Journal of Wind Engineering and Industrial Aerodynamics 77–78, 315–326.

Lanchaster, F.W., 1907. Aerodynamics. A. Constable&Co., London.

Luo, S.C., Chew, Y.T., Ng, Y.T., 2003. Hysteresis phenomenon in the galloping oscillation of a square cylinder. Journal of Fluids and Structures 18, 103–118.

Murdock, J.A., 1991. Perturbations, Theory and Methods. Wiley, New York.

Nakamura, Y., Matsukawa, T., 1987. Vortex excitation of rectangular cylinder with a long side normal to the flow. Journal of Fluid Mechanics 180, 171–191.

Novak, M., 1969. Aeroelastic galloping of prismatic bodies. ASCE Journal Engineering Mechanics Division 96, 115–142.

Novak, M., 1972. Galloping oscillations of prismatic structures. ASCE Journal Engineering Mechanics Division 98, 27–46.

Novak, M., Tanaka, H., 1974. Effect of turbulence on galloping instability. ASCE Journal Engineering Mechanics Division 100, 27–47.

Parkinson, G.V., 1961. On the aeroelastic instability of bluff cylinders. Journal of Applied Mechanics 28, 252–258.

Parkinson, G.V., 1964. The square prism as an aeroelastic nonlinear oscillator. Quarterly Journal Mechanics and Applied Mathematics 17, 225–239.

Rockwell, D., Naudascher, E., 1994. Flow-Induced Vibrations, An Engineering Guide. Dover Publications, Mineola.

Simpson, A., 1972. Determination of the natural frequencies of multi-conductor overhead transmission lines. Journal of Sound and Vibration 20, 417–449.

Sisto, F., 1953. Stall flutter in cascades. Journal of the Aeronautical Sciences 20, 598–604.

Van Oudheusden, B.W., 2000. Aerodynamic stiffness and damping effects in the rotational galloping of a rectangular cross-section. Journal of Fluids and Structures 14, 1119–1144.